ANTIVIRAL IMMUNITY

Type I interferons instigate fetal demise after Zika virus infection

Laura J. Yockey,[1] Kellie A. Jurado,[1] Nitin Arora,[2] Alon Millet,[1] Tasfia Rakib,[1] Kristin M. Milano,[3] Andrew K. Hastings,[4] Erol Fikrig,[4,5] Yong Kong,[6] Tamas L. Horvath,[7] Scott Weatherbee,[8] Harvey J. Kliman,[3] Carolyn B. Coyne,[2,9] Akiko Iwasaki[1,5]*

Zika virus (ZIKV) infection during pregnancy is associated with adverse fetal outcomes, including microcephaly, growth restriction, and fetal demise. Type I interferons (IFNs) are essential for host resistance against ZIKV, and IFN-α/β receptor (IFNAR)–deficient mice are highly susceptible to ZIKV infection. Severe fetal growth restriction with placental damage and fetal resorption is observed after ZIKV infection of type I IFN receptor knockout (*Ifnar1*$^{-/-}$) dams mated with wild-type sires, resulting in fetuses with functional type I IFN signaling. The role of type I IFNs in limiting or mediating ZIKV disease within this congenital infection model remains unknown. In this study, we challenged *Ifnar1*$^{-/-}$ dams mated with *Ifnar1*$^{+/-}$ sires with ZIKV. This breeding scheme enabled us to examine pregnant dams that carry a mixture of fetuses that express (*Ifnar1*$^{+/-}$) or do not express IFNAR (*Ifnar1*$^{-/-}$) within the same uterus. Virus replicated to a higher titer in the placenta of *Ifnar1*$^{-/-}$ than within the *Ifnar1*$^{+/-}$ concepti. Yet, rather unexpectedly, we found that only *Ifnar1*$^{+/-}$ fetuses were resorbed after ZIKV infection during early pregnancy, whereas their *Ifnar1*$^{-/-}$ littermates continue to develop. Analyses of the fetus and placenta revealed that, after ZIKV infection, IFNAR signaling in the conceptus inhibits development of the placental labyrinth, resulting in abnormal architecture of the maternal-fetal barrier. Exposure of midgestation human chorionic villous explants to type I IFN, but not type III IFNs, altered placental morphology and induced cytoskeletal rearrangements within the villous core. Our results implicate type I IFNs as a possible mediator of pregnancy complications, including spontaneous abortions and growth restriction, in the context of congenital viral infections.

INTRODUCTION

Zika virus (ZIKV), an emerging mosquito-borne flavivirus, infected more than 500,000 individuals in 2015 and 2016 as it spread across the Americas and is now present in 62 countries across the world (*1*, *2*). Symptoms in healthy individuals are mostly mild, including fever, rash, and conjunctivitis, with most infections remaining asymptomatic. However, the recent outbreak has led to a worldwide concern over the ability of the virus to cause birth defects, including microcephaly, in infected pregnant women. In addition to microcephaly, ZIKV causes a range of other pregnancy complications, including intrauterine growth restriction (IUGR), spontaneous abortion, and stillbirth (*3*). Although ZIKV is primarily transmitted through the mosquito *Aedes aegypti*, increasing evidence supports sexual transmission as a route of infection: ZIKV RNA persists in semen for up to 6 months after infection, and there are a number of reports of ZIKV transmission among sexual partners in areas where mosquito transmission has not been reported (*4*, *5*). However, it is unknown whether the mechanisms of ZIKV-induced fetal pathology after mosquito-borne and sexually transmitted infection are similar.

The type I interferons (IFNs), including IFN-β and multiple subtypes of IFN-α, are key antiviral factors that mount a rapid and potent innate defense against viruses (*6*). Production of type I IFN is initiated through recognition of pathogen-associated molecular patterns, generated during viral infection (*7*, *8*). Type I IFNs bind to their receptor, IFNAR (IFN-α/β receptor), to induce an antiviral state through transcription of IFN-stimulated genes (ISGs), which restrict viral replication through a broad range of antiviral mechanisms (*6*, *9*). In addition to inducing cell-intrinsic antiviral effects, IFNs have an extensive range of biological activities, including activating adaptive immune responses (*10*), blocking cell proliferation, and inducing apoptosis (*11*). Thus, in addition to restricting viral infection, IFNs also have the potential to contribute to pathogenesis.

Multiple mouse models of ZIKV infection have demonstrated adverse pregnancy outcomes (*12*–*16*). Because ZIKV is unable to suppress the mouse IFNAR signaling as successfully as it suppresses human IFNAR signaling (*17*, *18*), many mouse models of ZIKV infection require blockade of IFNAR using an antibody, use of *Ifnar1*-deficient mice, or the use of high levels of virus to induce pathology (*12*, *14*, *19*). Pregnancy studies of ZIKV have used a model in which *Ifnar1*$^{-/-}$ females are crossed to wild-type (WT) males, creating *Ifnar1*$^{+/-}$ fetuses with an intact IFN response (*13*, *14*, *20*). In these models, fetuses develop severe growth restriction when pregnant dams are infected subcutaneously or intravaginally after embryonic day 7.5 (E7.5). If mice are infected earlier, between E4.5 and E6.5, most fetuses are resorbed. ZIKV infection in this model induces severe pathology of the placenta and abnormal placental architecture (*13*).

The placenta supports fetal development by facilitating exchange of nutrients and gases between the maternal and fetal blood. In addition, it serves as a barrier by preventing transfer of pathogens from the mother to the fetus (*3*, *21*). It is known that inflammation and infection can disrupt the function and development of the placenta, leading to IUGR, preeclampsia, preterm birth, and fetal demise, as demonstrated in humans and animal models (*22*, *23*). Others have

[1]Department of Immunobiology, Yale University School of Medicine, New Haven, CT 06520, USA. [2]Department of Pediatrics, University of Pittsburgh School of Medicine, Pittsburgh, PA 15224, USA. [3]Department of Obstetrics, Gynecology, and Reproductive Sciences, Yale University School of Medicine, New Haven, CT 06520, USA. [4]Section of Infectious Diseases, Department of Internal Medicine, Yale University School of Medicine, New Haven, CT 06520, USA. [5]Howard Hughes Medical Institute, Chevy Chase, MD 20815, USA. [6]Yale School of Public Health, New Haven, CT 06520, USA. [7]Program in Integrative Cell Signaling and Neurobiology of Metabolism, Section of Comparative Medicine New Haven, CT 06520, USA. [8]Department of Genetics, Yale University School of Medicine, New Haven, CT 06520, USA. [9]Center for Microbial Pathogenesis, Children's Hospital of Pittsburgh of UPMC (University of Pittsburgh Medical Center), Pittsburgh, PA 15224, USA.
*Corresponding author. Email: akiko.iwasaki@yale.edu

also suggested that the immune response to ZIKV at the maternal-fetal interface may be responsible for ZIKV-associated birth defects (*24*). In addition, type I IFNs have been shown to mediate preterm birth in mouse models (*25*). On the other hand, IFNs are known to have important roles in supporting normal pregnancy and protecting the fetus from viral infections (*26*). For example, ISGs are up-regulated during implantation in mice and humans (*27*), and human syncytiotrophoblasts constitutively express type III IFNs (IFN-λs), making them resistant to infection by viruses (*28*, *29*). In addition, type III IFNs play a role in restricting ZIKV vertical transmission in mice (*20*).

In this study, we interrogate the effect of type I IFN signaling on fetal development using a mouse model of ZIKV infection. Vaginal or subcutaneous ZIKV infection of *Ifnar1*$^{-/-}$ dams crossed with *Ifnar1*$^{+/-}$ sires enabled us to investigate the role of IFNAR signaling in antiviral protection and disease. Paradoxically, our results revealed a detrimental role of fetal IFNAR signaling in mediating IUGR and fetal resorption by causing abnormal placental development.

RESULTS

Fetal IFNAR signaling instigates fetal demise despite controlling ZIKV replication

In our previous studies, we observed that vaginal infection of mice lacking the transcription factors upstream of type I IFN, *Irf3*$^{-/-}$ *Irf7*$^{-/-}$ dams crossed to *Irf3*$^{-/-}$ *Irf7*$^{-/-}$ sires, had higher levels of ZIKV in the placenta but had minimal growth restriction compared with fetuses from *Ifnar*$^{-/-}$ dams crossed to WT sires (*14*). Although the *Irf3*$^{-/-}$ *Irf7*$^{-/-}$ mice are capable of responding to IFN, we hypothesize that the lack of pathology in this model, despite high levels of virus, is due to the lack of IFN induction in the first place. Consistent with this, we observed that the ISGs were induced in *Ifnar*$^{+/-}$ fetuses and placenta, but they were absent in the *Irf3*$^{-/-}$ *Irf7*$^{-/-}$ matings, correlating with the level of pathology (fig. S1, A to F). These findings led us to hypothesize that IFN signaling, rather than the levels of virus, mediates fetal pathology after ZIKV infection.

To directly test the role of type I IFNs in antiviral defense and fetal development after ZIKV infection, we crossed *Ifnar1*$^{-/-}$ females with *Ifnar1*$^{+/-}$ males, producing a mixture of *Ifnar1*$^{-/-}$ and *Ifnar1*$^{+/-}$ fetuses in the same litter (Fig. 1A). Pregnant dams were infected intravaginally with 1.5×10^5 plaque-forming units (PFU) of Cambodian strain of ZIKV on either E5.5 or E.8.5, corresponding to the mid and late first trimester in humans (*30*), respectively. Fetuses were harvested on E17.5, close to term. We observed resorption of all fetuses of the *Ifnar1*$^{+/-}$ genotype when dams were infected with ZIKV on E5.5 (Fig. 1, B and C). However, all *Ifnar1*$^{-/-}$ littermates continued to develop after infection on E5.5, indicating that a functional copy of *Ifnar1* is required to mediate fetal demise after early ZIKV infection of pregnant dams (Fig. 1, B and C). When dams were challenged with ZIKV on E8.5, *Ifnar1*$^{+/-}$ fetuses were not resorbed but showed more severe growth restriction compared with their *Ifnar1*$^{-/-}$ littermates (Fig. 1, B and C). Analysis of viral RNA showed that, after E8.5 infection, there was more viral RNA detected in the placentas of the *Ifnar1*$^{-/-}$ littermates compared with their *Ifnar1*$^{+/-}$ littermates on E17.5 [9 days postinfection (dpi)] (Fig. 1D). Plaque assays revealed 1000-fold higher levels of infectious virus in the *Ifnar*$^{-/-}$ placentas compared with *Ifnar*$^{+/-}$ placentas (fig. S2A). After infection at E5.5, there were comparable levels of virus in the *Ifnar1*$^{-/-}$ placenta and the resorbed *Ifnar1*$^{+/-}$ conceptus, and these levels were lower than what was observed for the E8.5 *Ifnar1*$^{-/-}$ placentas on E17.5 (12 dpi) (Fig. 1D). In the fetus, viral RNA was present but at low levels in both genotypes and at both time points of infection (Fig. 1E), and infectious virus was below the limit of detection for most fetuses after infection at E8.5 (fig. S2B). These results indicated that IFNAR signaling in the conceptus, despite controlling ZIKV replication in the placenta, leads to fetal demise after congenital infection.

To understand how and when development is blocked in the *Ifnar1*$^{+/-}$ conceptus, we harvested fetuses at various days after infection of dams on E5.5. Gross examination of the *Ifnar1*$^{+/-}$ fetuses revealed no overt differences with *Ifnar1*$^{-/-}$ fetuses or with uninfected counterparts on E9.5 (Fig. 2, A and B). On E10.5, there was a modest reduction in size of the *Ifnar1*$^{+/-}$ fetuses, and in 1 of 6 litters, all *Ifnar1*$^{+/-}$ fetuses were resorbed (3 of 17), but fetuses otherwise appeared grossly normal (Fig. 2, A and B). However, by E11.5, the majority of *Ifnar1*$^{+/-}$ fetuses (7 of 11) were dead, and by E12.5, all *Ifnar1*$^{+/-}$ fetuses were resorbed (Fig. 2, A and B). Thus, IFNAR-dependent fetal demise after early ZIKV infection occurs between E10.5 and E12.5.

Placental labyrinth architecture is abnormal in IFNAR-competent concepti

Postimplantation death between E5.5 and E12.5 is typically caused by defects in the fetal red blood cells (RBCs), vasculature, heart, or the placenta (*31*). Thus, we focused on analysis of the placenta, which develops between E8.5 and E10.5 (*32*, *33*). Global transcriptional analysis by RNA sequencing (RNA-seq) of placentas at E10.5 demonstrated evidence of active IFNAR signaling in the *Ifnar1*$^{+/-}$ placenta, with robust induction of hundreds of ISGs (fig. S3 and table S2). To determine which cells are infected by ZIKV, we stained the E10.5 placenta and decidua for ZIKV antigen. The decidua is the maternally derived endometrial lining of the uterus, and the fetus-derived placenta is composed of the junctional zone and labyrinth zone, where nutrient exchange occurs between the maternal and fetal blood (Fig. 3A) (*21*, *32*). We detected rare ZIKV-infected leukocytes (CD45$^+$ cells) in both the *Ifnar1*$^{+/-}$ and *Ifnar1*$^{-/-}$ decidua but not in the underlying placenta (fig. S4). These cells likely represent decidual macrophages or dendritic cells, and this is consistent with a report showing ZIKV RNA in leukocytes of maternal tissue surrounding the placenta in an infected patient (*34*, *35*). These results suggest that ZIKV infects maternal cells in the decidua, which may be a source of type I IFNs that act on fetal cells of the underlying junctional zone or labyrinth layer to induce robust ISGs.

Next, we performed histological analysis of the developing placenta and decidua to determine the impact of ISG expression. At E9.5, the placenta and decidua were grossly normal in all groups: They showed normal decidualization, a layer of trophoblast giant cells, and a labyrinth with both maternal blood spaces, containing anucleated maternal RBCs, and fetal blood spaces, containing nucleated fetal RBCs (fig. S5). By E10.5, we observed marked abnormality in the labyrinth of the ZIKV-infected *Ifnar1*$^{+/-}$, but not *Ifnar1*$^{-/-}$, placentas (Fig. 3B). Specifically, the labyrinth appeared to have denser cellularity, with decreased vascular spaces and minimal fetal blood cell content (Fig. 3B, arrows). In addition, there were abnormal spheroid structures (Fig. 3B, asterisk), likely composed of trophoblasts. The decidua and trophoblast giant cells were comparable between all groups. Although the labyrinth of the infected *Ifnar1*$^{-/-}$ placentas looked more disorganized with increased cellularity compared with the uninfected controls, there were still abundant fetal RBCs within the fetal blood space (Fig. 3B). By E11.5, when most ZIKV-infected *Ifnar1*$^{+/-}$ fetuses were resorbed, the labyrinth appeared disorganized with reduced fetal blood vessels and abundant spheroid structures, and by E12.5, *Ifnar1*$^{+/-}$ placentas show almost no maternal or fetal blood vessels (fig. S5). In contrast, the labyrinths of *Ifnar1*$^{-/-}$ placentas on E11.5 and E12.5 were

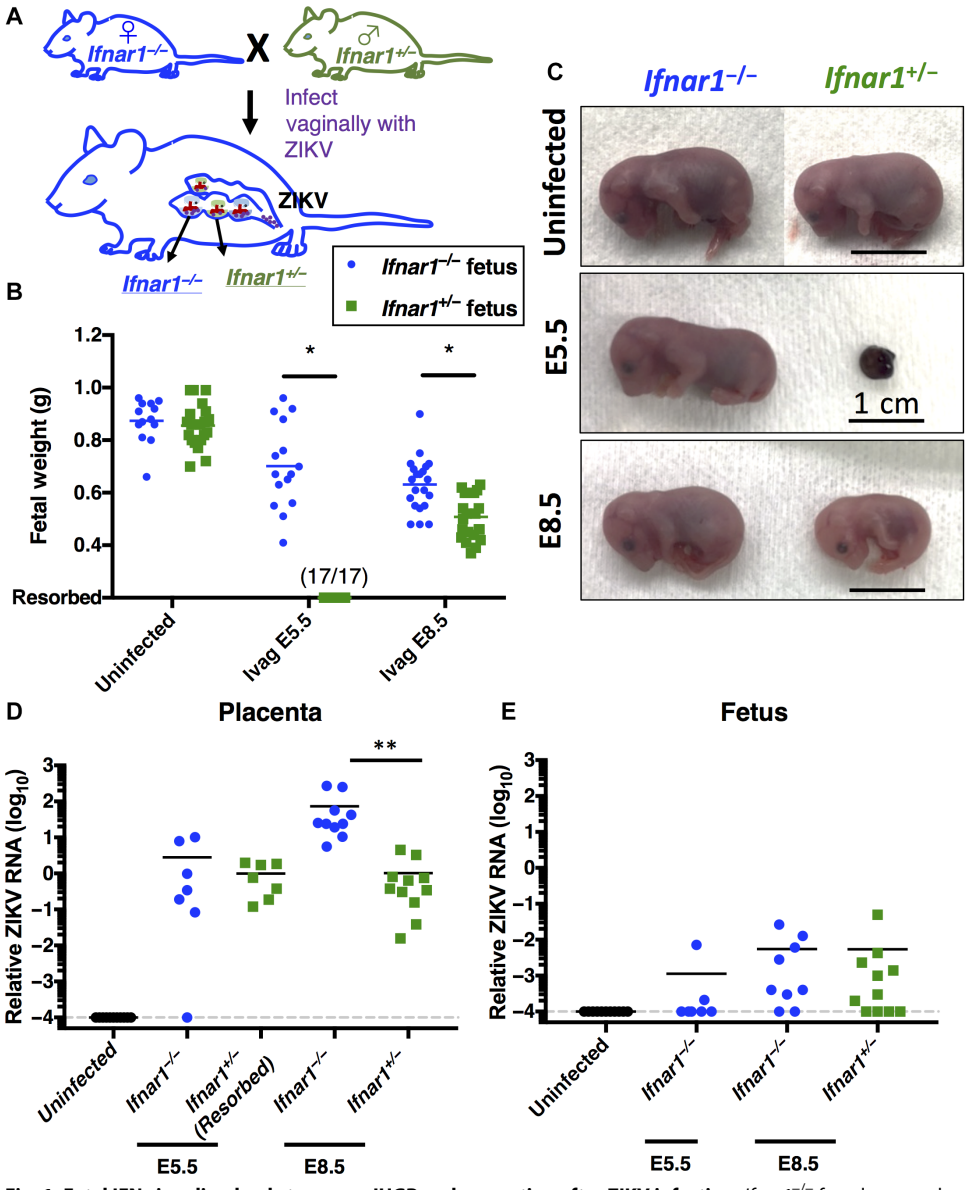

Fig. 1. Fetal IFN signaling leads to severe IUGR and resorption after ZIKV infection. *Ifnar1*$^{-/-}$ females mated to *Ifnar1*$^{+/-}$ males were infected intravaginally (Ivag) with 1.5×10^5 PFU Cambodian ZIKV on E5.5 or E8.5 and harvested on E17.5. (**A**) Schematic showing mating strategy. Fetal weights were measured (**B**), and fetuses were visually inspected (**C**). RNA was isolated from the placenta or resorbed conceptus (**D**) or fetus (**E**) to determine ZIKV levels. Relative ZIKV levels were determined by normalization to *Hprt*. Individual data points with mean are shown. For fetal weights, ZIKV E5.5 ($n = 15$ *Ifnar1*$^{-/-}$ and $n = 17$ *Ifnar1*$^{+/-}$ from four litters); ZIKV E8.5 ($n = 21$ *Ifnar1*$^{-/-}$ and $n = 22$ *Ifnar1*$^{+/-}$ from six litters); and uninfected ($n = 13$ *Ifnar1*$^{-/-}$ and $n = 21$ *Ifnar1*$^{+/-}$ from four litters). For ZIKV RNA, ZIKV E5.5 ($n = 7$ *Ifnar1*$^{-/-}$ and $n = 7$ *Ifnar1*$^{+/-}$ from three litters); ZIKV E8.5 ($n = 9$ to 10 *Ifnar1*$^{-/-}$ and $n = 11$ *Ifnar1*$^{+/-}$ from five litters); and uninfected ($n = 11$ from three litters with both genotypes pooled). Data are pooled from at least two independent experiments from each infection time point. Scale bars, 1 cm. *$P < 0.05$ and ** $P < 0.01$ by Tukey's multiple comparison test.

indistinguishable from those of the uninfected controls with abundant adjacent fetal and maternal blood spaces (fig. S5). These results suggested that type I IFN induced in response to ZIKV interferes with development of fetal vasculature in the placenta labyrinth.

To examine this possibility, we stained tissue sections of E10.5 placentas from dams infected on E5.5 with cytokeratin (CK) to label trophoblasts and CD31 to label blood vessels. We observed a network of closely associated CD31$^+$ (endothelial cell demarcating fetal blood space) and CK-positive (trophoblast demarcating maternal blood space) structures in both uninfected and ZIKV-infected *Ifnar1*$^{-/-}$ placentas (Fig. 3C). In contrast, CD31 staining in the ZIKV-infected *Ifnar1*$^{+/-}$ placentas was markedly reduced, wherein the limited CD31$^+$ cells were found on the edge of the placental structure devoid of luminal spaces (Fig. 3C). Immunohistochemistry staining of the placentas with anti-CD31 antibody confirmed the collapsed vasculature and reduced number of the fetal endothelial cells (fig. S6A). Anti–E-cadherin antibody, which stains the trophoblasts, revealed that many of the densely packed cells in the E10.5 placenta were Ecad$^+$ trophoblasts (fig. S6B). These results indicate that defective development of fetal vasculature and abnormal trophoblasts in the labyrinth immediately precede the death of the IFNAR-intact fetus after ZIKV infection of pregnant dams.

IFNAR signaling leads to increased apoptosis in the placental labyrinth, an abnormal maternal-fetal barrier, and fetal hypoxia

On the basis of the known functions of type I IFNs, we hypothesized that IFNAR signaling in the fetus inhibits placental development through three possible mechanisms: inducing immune cell recruitment and invasion of the labyrinth, blocking cellular proliferation, or inducing cell death (*10*, *11*). At E10.5, CD45$^+$ leukocytes were restricted to the decidua in all groups and did not infiltrate the CK-positive junctional zone or the labyrinth (fig. S6C), ruling out inflammatory leukocyte infiltration as the mechanism of fetal demise. Next, we examined cell proliferation in the labyrinth by Ki67 staining. All placentas showed abundant Ki67$^+$ cells at E10.5 (Fig. 4A), excluding the role of IFNAR signaling in blocking cell proliferation as the mechanism of fetal demise. To examine whether IFNAR signaling is inducing cell death, we stained for activated (cleaved) caspase-3 (Casp3) as a marker of apoptotic cells. There was no Casp3-positive staining in the labyrinth of the uninfected placentas or infected *Ifnar1*$^{-/-}$ placentas at E10.5 (Fig. 4B). In contrast, in the infected *Ifnar1*$^{+/-}$ placenta, we detected Casp3 staining in the labyrinth in a pattern consistent with the endothelial cells, fetal blood cells, or adjacent trophoblasts surrounding the spheroid structure (Fig. 4B). These results are consistent with a previous report (*13*) and suggest a role for IFNAR in mediating apoptosis of fetal

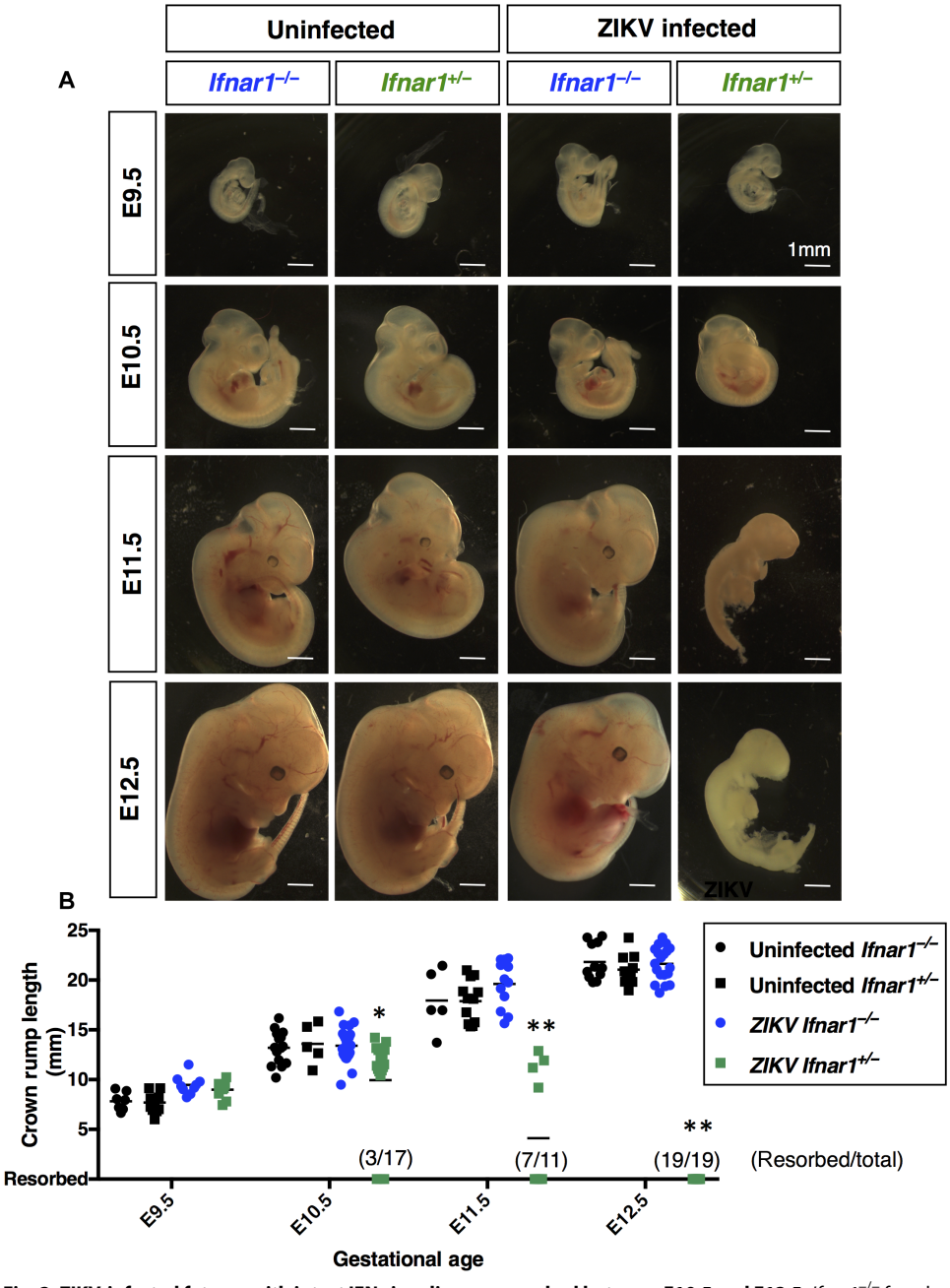

Fig. 2. ZIKV-infected fetuses with intact IFN signaling are resorbed between E10.5 and E12.5. *Ifnar1*$^{-/-}$ females mated to *Ifnar1*$^{+/-}$ males were infected intravaginally with 1.5×10^5 PFU Cambodian ZIKV at E5.5 and harvested at indicated time points. (**A**) Representative images of three to five litters for infected and two to three litters for uninfected are shown per time point. Scale bars, 1 mm. (**B**) Crown-rump length was measured by tracing distance from crown of head to end of tail using ImageJ. Means with individual points are graphed. Data points shown represent the following: E9.5 uninfected *Ifnar1*$^{-/-}$ ($n = 7$) and *Ifnar1*$^{+/-}$ ($n = 12$ from two litters) and infected *Ifnar1*$^{-/-}$ ($n = 9$) and *Ifnar1*$^{+/-}$ ($n = 10$ from three litters); E10.5 uninfected *Ifnar1*$^{-/-}$ ($n = 15$) and *Ifnar1*$^{+/-}$ ($n = 5$ from three litters) and infected *Ifnar1*$^{-/-}$ ($n = 24$) and *Ifnar1*$^{+/-}$ ($n = 17$ from six litters); E11.5 uninfected *Ifnar1*$^{-/-}$ ($n = 5$) and *Ifnar1*$^{+/-}$ ($n = 12$ from three litters) and infected *Ifnar1*$^{-/-}$ ($n = 12$) and *Ifnar1*$^{+/-}$ ($n = 11$ from three litters); E12.5 uninfected *Ifnar1*$^{-/-}$ ($n = 11$) and *Ifnar1*$^{+/-}$ ($n = 11$ from three litters) and infected *Ifnar1*$^{-/-}$ ($n = 19$) and *Ifnar1*$^{+/-}$ ($n = 19$ from five litters). Data are pooled from at least two independent experiments from each infection time point. *$P < 0.05$ and **$P < 0.0001$ compared with all other groups by Tukey's multiple comparison test. No significant differences were found between other groups.

endothelial cells and trophoblasts as an underlying mechanism of placental dysfunction.

To examine the abnormal placenta architecture at a cellular level, we performed electron microscopy to analyze the maternal-fetal interface on E10.5. In the uninfected placentas and infected *Ifnar1*$^{-/-}$ placentas, the expected trilaminar interhemal barrier was seen, with anucleated maternal blood (mrbc) and nucleated fetal blood (frbc) being separated by four layers of cells: the sinusoidal trophoblast giant cell (stgc) that directly contacts the maternal blood, two continuous syncytial layers of trophoblast that are closely connected (ST-I and ST-II), and a layer of endothelial cells (ec) that directly contact the fetal blood (Fig. 4C) (*32*, *36*). ST-I and ST-II were tightly adhered to one another (Fig. 4C, arrows). There was no mixing between maternal and fetal blood in the uninfected placenta. In the infected *Ifnar1*$^{+/-}$ placentas, there were multiple instances of mixing between the maternal and fetal blood in the labyrinth (Fig. 4C). When separated maternal and fetal circulations were found, the barrier between the two was highly abnormal, with no evidence of the normal four-cell layer barrier and breakdown between cells making the maternal-fetal barrier (Fig. 4C). Thus, IFNAR signaling in the placenta leads to an abnormal maternal-fetal blood barrier with local breakdown.

On the basis of the findings of an abnormal vasculature in the placental labyrinth and abnormal maternal-fetal barrier, we examined the transcriptional changes in the fetus to examine whether lack of adequate gas exchange between mother and fetus may be contributing to fetal demise. We found that hypoxia response genes, including *Vegfa*, *Adm*, *Bnip3*, *Glut1*, and *Pfkfb3*, were all significantly upregulated in the ZIKV-infected *Ifnar1*$^{+/-}$ fetuses relative to uninfected controls and to their infected *Ifnar1*$^{-/-}$ littermates (Fig. 5, A to E) (*37*, *38*). Thus, the death of the *Ifnar1*$^{+/-}$ fetuses after ZIKV infection is preceded by hypoxia.

IFNAR signaling mediates fetal death after subcutaneous ZIKV infection and poly(I:C) treatment

To determine whether IFNAR signaling mediates fetal resorption after other routes of ZIKV infection and with other strains

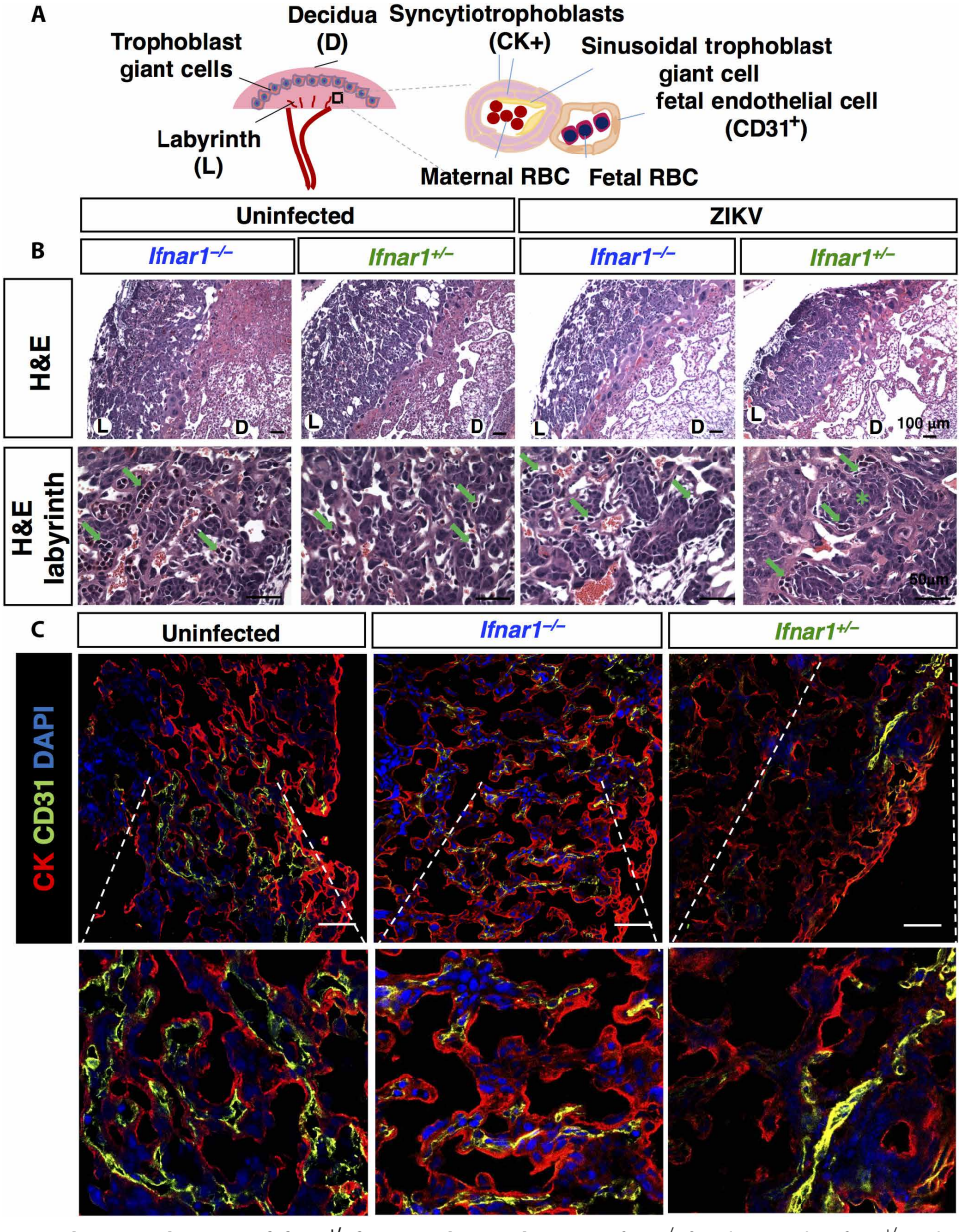

Fig. 3. Placenta architecture of *Ifnar1*$^{+/-}$ fetuses is disrupted at E10.5. *Ifnar1*$^{-/-}$ females mated to *Ifnar1*$^{+/-}$ males were infected intravaginally with 1.5×10^5 PFU Cambodian ZIKV at E5.5 and harvested at E10.5. (**A**) Schematic of decidua and placenta architecture and cell types. (**B**) Placentas were fixed in PFA, and paraffin-embedded sections were stained by H&E. Whole placenta and decidua (top) or magnified labyrinth (bottom) are shown. Representative images of 10 placentas/deciduas per genotype from five litters were analyzed for infected, and four placentas/deciduas per genotype per time point from two litters were analyzed for uninfected. Labyrinth, L, and decidua, D, are labeled with respective letters. The asterisk indicates abnormal spheroid structure. Arrows indicate fetal RBCs. Scale bars, 100 μm (top) and 50 μm (bottom). (**C**) PFA-fixed frozen sections from infected littermates were costained for CK (red, trophoblasts), CD31 (green, blood vessels), and DAPI (blue). Representative images from at least three placentas per genotype from at least two litters are shown. Scale bars, 75 μm.

of ZIKV, we challenged *Ifnar1*$^{-/-}$ females crossed with *Ifnar1*$^{+/-}$ males subcutaneously with the Brazilian strain of ZIKV on E6.5 (*13*). After challenging with a high dose (3.4×10^5 PFU) of ZIKV, most *Ifnar1*$^{+/-}$ fetuses were resorbed by E12.5, but *Ifnar1*$^{-/-}$ fetuses continued to develop (fig. S7, A and B). To analyze fetal development at later time points without maternal lethality, we challenged *Ifnar1*$^{-/-}$ females mated with *Ifnar1*$^{+/-}$ males with a sublethal dose of ZIKV (1×10^3 PFU) subcutaneously at E6.5 and harvested the fetuses at E17.5. Again, similar to the vaginal ZIKV infection, all *Ifnar1*$^{+/-}$ fetuses were resorbed, but *Ifnar1*$^{-/-}$ fetuses were grossly normal (fig. S7, C and D). Thus, IFNAR-dependent fetal resorption occurs after subcutaneous and intravaginal ZIKV challenge, with both Brazilian and Cambodian ZIKV strains.

To examine whether IFNAR signaling is sufficient to induce fetal resorption independent of ZIKV infection, we challenged mice with polyinosinic/polycytidylic acid [poly(I:C)], a double-stranded RNA viral mimic capable of eliciting robust type I IFN responses (*39*). After intraperitoneal injection of 200 μg of poly(I:C) at E7.5, all fetuses of WT females mated with WT males were resorbed by E9.5, and we could not recover any fetal material in five of six injected females by E10.5, consistent with previous reports (Fig. 6, A and C) (*40*). When we challenged *Ifnar1*$^{-/-}$ females crossed with *Ifnar1*$^{+/-}$ males with poly(I:C) on E7.5, the majority of both *Ifnar1*$^{-/-}$ and *Ifnar1*$^{+/-}$ fetuses continued to develop as examined on E10.5 and E12.5 (Fig. 6, B and C). Thus, maternal IFNAR signaling was necessary for mediating poly(I:C)-induced fetal resorption.

Type I IFN (but not type III IFN) treatment of human midgestation villous explants leads to deformation

To determine the impact of type I IFNs on the human placenta, we treated midgestation (19 to 23 weeks) human chorionic villous explants with a type I IFN, recombinant IFN-β, or a type III IFN, recombinant IFN-λ3. Isolated villi were treated with recombinant IFN within hours after their isolation, when their structure and morphology remained completely intact, as characterized by a continuous layer of CK-positive trophoblasts covering the surfaces of the isolated villi [Fig 7, A (left) and B (top)]. After ~16 to 20 hours of treatment, the architecture of IFN-β–treated villi became markedly abnormal, with areas of aggregated nuclei formed at the distal end of villi treated with IFN-β (either 100 or 1000 U) [Fig. 7, A (arrows) to C]. In contrast, treatment of the villous explants with IFN-λ3 showed no gross impact (Fig. 7, A and C). The abnormal villous structures resembled syncytial knots, which are associated with pathological states of pregnancy; sprouts, which represent overproliferation of the syncytiotrophoblast layer; or apoptotic shedding

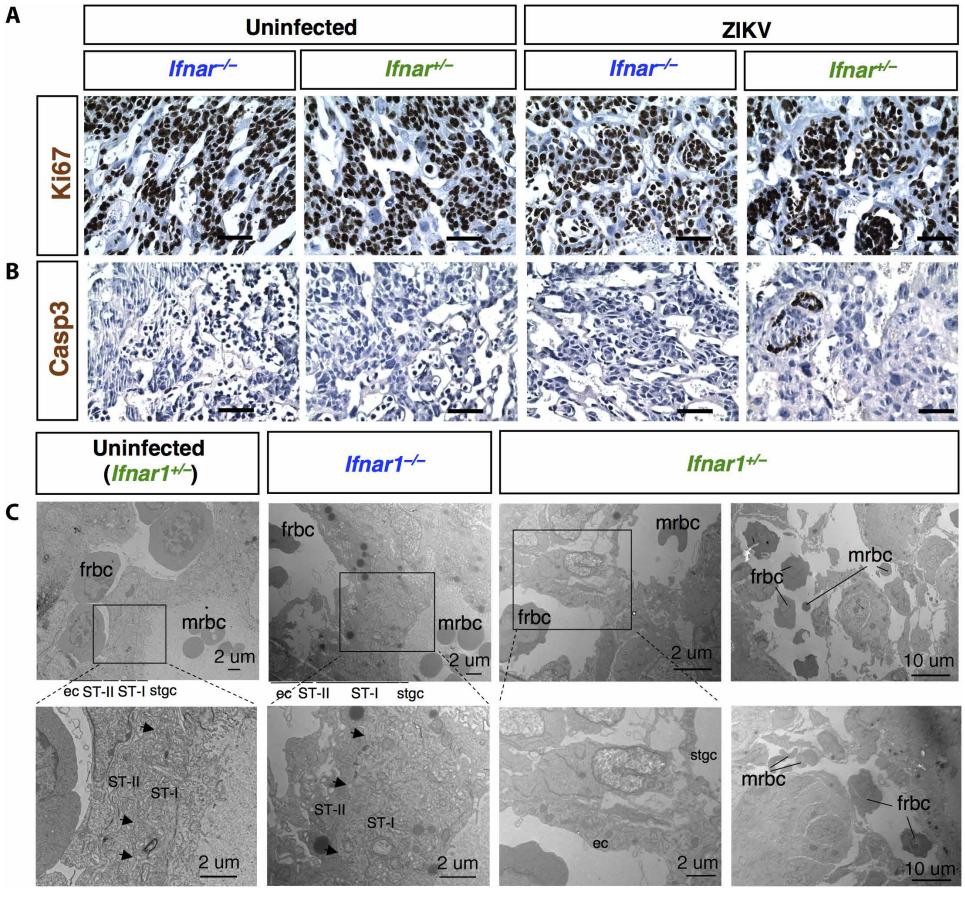

Fig. 4. *Ifnar1*$^{+/-}$ placentas show increased apoptosis and abnormal maternal-fetal blood barrier. *Ifnar1*$^{-/-}$ females mated to *Ifnar1*$^{+/-}$ males were infected intravaginally with 1.5×10^5 PFU Cambodian ZIKV at E5.5 and harvested at E10.5. Paraffin-embedded sections were stained for Ki67 (**A**, dividing cells) or cleaved Casp3 (**B**, apoptotic cells) with DAB. From (A) and (B), images from labyrinth are shown. Scale bars, 50 μm. Representative images from at least three placentas/deciduas per condition from at least two litters are shown. (**C**) Placentas were fixed at least 24 hours in formaldehyde with 2.5% glutaraldehyde at 4°C. The labyrinth was dissected and processed for electron microscopy. Uninfected *Ifnar1*$^{+/-}$ labyrinth shows four layers of cells between frbc and mrbc: fetal endothelial cell (ec), two syncytiotrophoblast layers (ST-II, ST-I), and the sinusoidal trophoblast giant cell (stgc). Infected *Ifnar1*$^{-/-}$ placenta is similar to the uninfected control. The barrier between maternal and fetal blood of ZIKV-infected *Ifnar1*$^{+/-}$ placentas is highly abnormal with unfused cells (left). ZIKV-infected *Ifnar1*$^{+/-}$ shows multiple examples of mixing between maternal and fetal blood (right). Scale bars, 2 or 10 μm as labeled on the image. Multiple sections and planes from one placenta per condition were analyzed.

(*41*, *42*). In addition to the formation of syncytial knot– or sprout-like structures, we noted that IFN-β–treated villi also exhibited alterations in the actin cytoskeleton within the core of the villi as characterized by actin filament disassembly, suggesting widespread damage to the villi (Fig. 7D, bottom). To examine the global transcriptional changes in response to IFN-β and IFN-λ3 treatment, we performed whole-genome RNA-seq on villi treated with IFN-β or IFN-λ isolated from three different placental preparations. We found that both IFN-β and IFN-λ treatment induced significant transcriptional changes (273 and 101 total genes, respectively; $P < 0.05$) as illustrated by MA plots (Fig. 8A). However, we found that there was little overlap between the genes induced by IFN-β and IFN-λ exposure—whereas IFN-β treatment induced the up-regulation of the majority of transcripts (260 of 273), IFN-λ treatment correlated with the down-regulation of the majority of transcripts (89 of 101) (Fig. 8B). Consistent with this differential expression pattern, only 12 transcripts were differentially expressed by both IFN-β and IFN-λ treatment (Fig. 8C). We found that whereas IFN-β treatment induced many known ISGs, IFN-λ treatment had little impact on ISG expression (Fig. 8, D to F). In addition, consistent with the significant morphologic alterations of villous architecture induced by IFN-β treatment, IFN-β–treated villi exhibited suppression (by ~4-fold, $P = 0.04$) in the expression of the β chain of human chorionic gonadotropin, which is exclusively produced by syncytiotrophoblasts and is associated with placental function. Collectively, these data suggest that type I IFN is sufficient to induce morphological alterations and also possibly adversely affect placental function in the human developing placental villi.

DISCUSSION

Our findings highlight the detrimental impact of type I IFNs on the developing placenta and fetus by demonstrating that only the fetuses with a functional copy of IFNAR are resorbed after ZIKV infection. IFNAR signaling in the conceptus leads to abnormal placenta labyrinth development with apoptosis in the labyrinth, impaired fetal endothelial development, and disrupted maternal-fetal blood barrier. IFNAR signaling was important in controlling viral replication in the placenta. Despite this, IFNAR-mediated pathology outweighed the benefit of IFNAR-dependent control of viral replication. How exactly IFNAR signaling leads to the observed labyrinth pathology is unknown. The hypoxic state of the IFNAR-sufficient fetus, likely resulting from the fetal endothelial disruption, suggests an impaired delivery of oxygen and possibly nutrients being the underlying cause of fetal demise. Our results do not rule out a role for the direct action of ZIKV in mediating certain aspects of pathology, such as microcephaly, ocular defects, or other neurological abnormalities, which we do not address in this study. Despite having a less severe phenotype than their *Ifnar*$^{+/-}$ littermates, *Ifnar*$^{-/-}$ mice did exhibit growth restriction compared with their uninfected counterparts, consistent with previous reports (*43*). This growth restriction may be due to poor maternal health, but it could also be indicative of IFNAR-independent causes of birth defects, including direct pathogenic effects of the virus infection or immune response unrelated to type I IFNs. One limitation to our study is that the host-pathogen interactions, including the suppression of host IFNAR signaling by ZIKV NS5 protein, are not preserved in mice. Thus, to what extent the mouse model recapitulates ZIKV infection and disease in humans is unknown. An additional limitation is that the structure and development of the

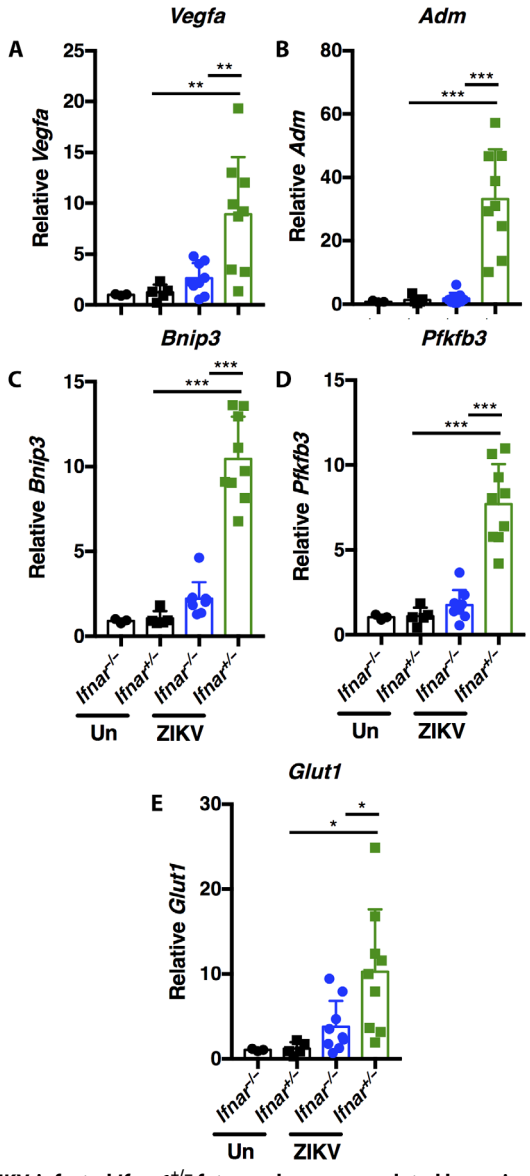

Fig. 5. ZIKV-infected *Ifnar1*$^{+/-}$ fetuses show up-regulated hypoxia response genes just before demise. *Ifnar1*$^{-/-}$ females mated to *Ifnar1*$^{+/-}$ males were infected intravaginally with 1.5×10^5 PFU Cambodian ZIKV at E5.5 and harvested at E10.5. RNA was extracted from fetuses, and expression of previously reported hypoxia-response genes *Vegfa* (**A**), *Adm* (**B**), *Bnip3* (**C**), *Pfkfb3* (**D**), and *Glut1* (**E**) analyzed by reverse transcription qPCR. Data represent $n = 9$ fetuses per genotype from three litters from ZIKV-infected litters and $n = 3$ *Ifnar1*$^{-/-}$ and $n = 5$ *Ifnar1*$^{+/-}$ fetuses from two uninfected litters. Data are pooled from at least two independent experiments per group. *$P < 0.05$, **$P < 0.01$, and ***$P < 0.0001$ by Tukey's multiple comparison test. Data were normalized to *Hprt* and represented as fold change over *Ifnar*$^{-/-}$ uninfected placentas.

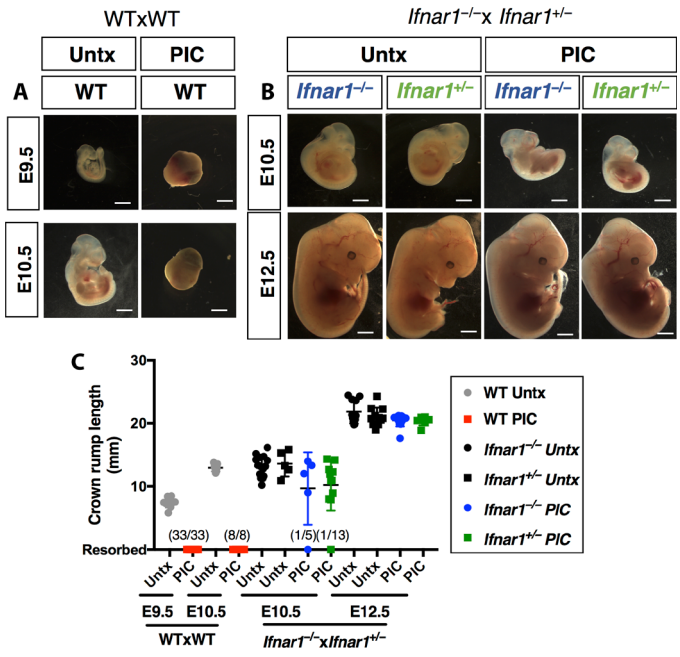

Fig. 6. Poly(I:C) injection of pregnant dams leads to fetal resorption in a maternal-IFNAR–dependent fashion. WT females mated to WT males (**A**) or *Ifnar1*$^{-/-}$ females mated to *Ifnar1*$^{+/-}$ males (**B**) were injected with 200-μg HMW poly(I:C) (PIC) at E7.5. Representative images from mice harvested between E9.5 and E12.5 are shown. Scale bars, 1 mm. (**C**) Crown-rump length was measured using ImageJ. Mean with SD and individual data points are shown. Data points represent the following: WTxWT litters untreated E9.5 ($n = 17$ from two litters), PIC E9.5 ($n = 33$ from four litters), untreated E10.5 ($n = 13$ from two litters), and PIC E10.5 ($n = 8$ from one litter); additional five injected litters showed no fetal remnants at time of harvest at E10.5. For *Ifnar1*$^{-/-}$x*Ifnar1*$^{+/-}$ litters, untreated E10.5 ($n = 15$ *Ifnar1*$^{-/-}$ and $n = 5$ *Ifnar1*$^{+/-}$ from three litters), PIC E10.5 ($n = 5$ *Ifnar1*$^{-/-}$ and $n = 11$ *Ifnar1*$^{+/-}$ from two litters), untreated E12.5 ($n = 11$ *Ifnar1*$^{-/-}$ and $n = 11$ *Ifnar1*$^{+/-}$ from three litters), and PIC E12.5 ($n = 13$ *Ifnar1*$^{-/-}$ and $n = 7$ *Ifnar1*$^{+/-}$ from two litters). Uninfected measurements for *Ifnar1*$^{-/-}$x*Ifnar1*$^{+/-}$ litters are the same as those shown in Fig.2B.

mouse placenta are significantly different from those of the human placenta, making it difficult to directly compare the pathological changes seen in the mouse placenta with those of humans.

To extend our findings to humans, we examined the impact of recombinant IFN-β on second-trimester villous explants. This experimental system allowed us to examine the impact of type I IFNs in the pre-existing syncytium and in a model that fully retains the architecture and multicellular composition of the human placenta. IFN-β exposure induced morphological changes in the human placenta, which correlated with alterations in syncytial and actin cytoskeletal architecture. Altered syncytial morphology resembled syncytial knots, a feature commonly associated with placentas of adverse pregnancy outcomes, including preeclampsia (*42*). Although common in full-term placentas, syncytial knots are rare in normal midgestation pregnancies (*44*). Given the short time scale over which they developed, they could also be apoptotic shedding of damaged cells. Our study required high levels (1000 U) of IFN-β to produce these effects, although we did note the appearance of syncytial knot–like structures at lower levels (100 U). It is difficult to assess whether this level of IFN may be present locally in congenital infections and what effects IFN-β may have over a longer period and during earlier stages of development, which were not possible to assess in this model. We found that treatment of villi with recombinant type III IFN, IFN-λ3, was not associated with the altered villous morphology or a strong ISG induction. These are consistent with previous reports that the syncytium constitutively produces IFN-λs (*28*) and may suggest that type III IFNs primarily function in an autocrine and paracrine manner to defend the developing fetus against viruses, as has been shown to occur in mice (*20*). Our data also showed that type I IFN, but not type III

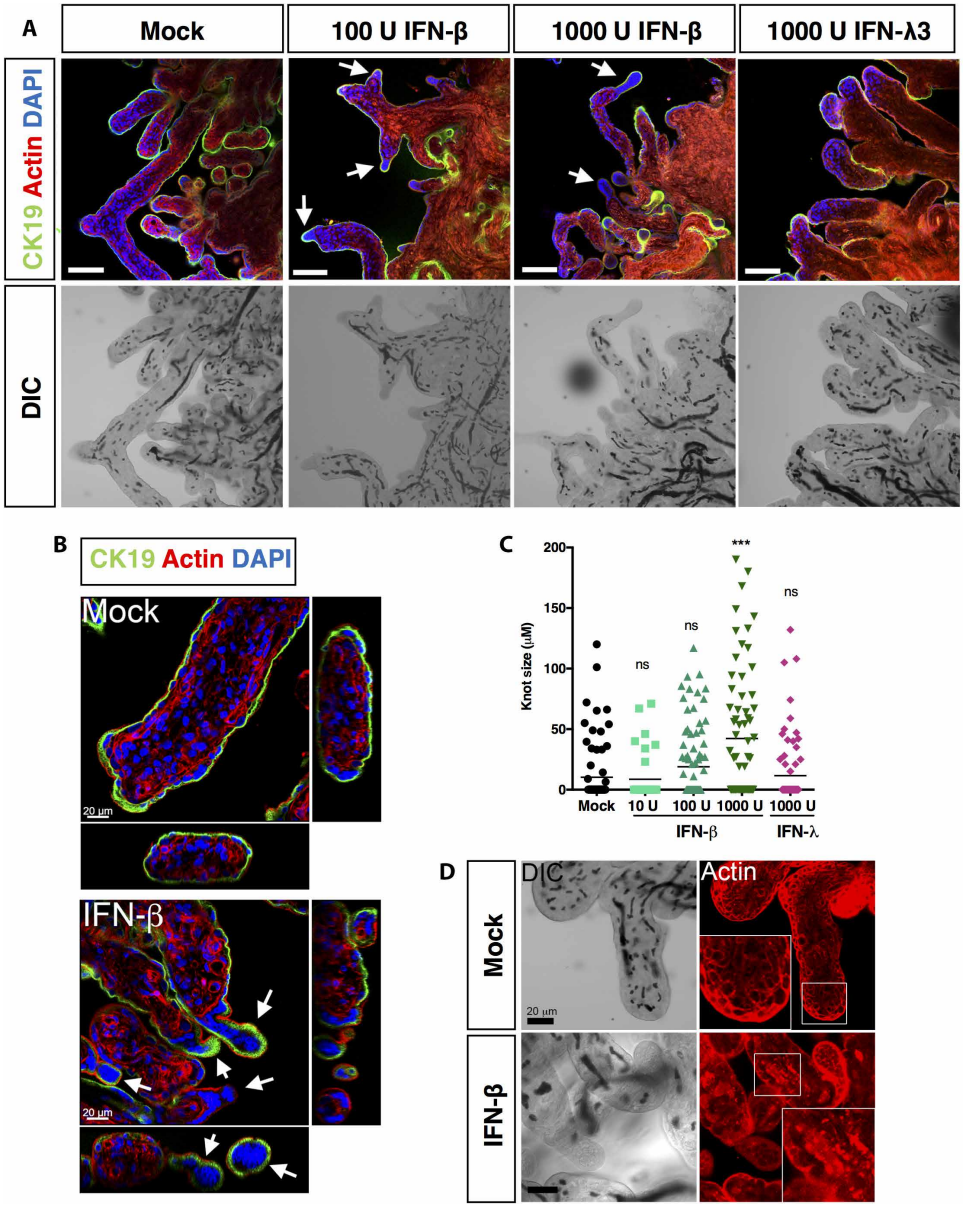

Fig. 7. IFN treatment of human midgestation villous explants induces syncytial knot formation. (**A**) Human midgestation (19 to 23 weeks) chorionic villi were isolated, placed in culture, and treated with 100 or 1000 U of recombinant human IFN-β or 1000 U of IFN-λ3 for ~16 to 20 hours. Villous explants were harvested, fixed in PFA, and stained for CK19 (green, trophoblasts) and actin (red). DAPI-stained nuclei are shown in blue and differential interference contrast (DIC) (bottom). Scale bars, 100 μm. Images are representative of villi isolated from four donors. Arrow indicates syncytial knot. (**B**) Three-dimensional image reconstruction of mock- or IFN-β (1000 U)–treated explants stained for CK19 (green) and actin (red). DAPI-stained nuclei are shown in blue. Scale bars, 20 μm. (**C**) Quantification of syncytial knot size using Imaris in villi treated with 10, 100, or 1000 U of IFN-β or 1000 U of IFN-λ3 for ~24 hours. Each symbol represents an individual villous from a total of three donors, and the black line represents the mean. ***$P <$ 0.001 by Dunnett's multiple comparison test to mock. ns, not significant. (**D**) Confocal micrographs of mock- or IFN-β (1000 U)–treated villi stained for actin (red, right). DIC is shown on the left. White box denotes zoomed area shown at the bottom left (mock) or right (IFN-β). Scale bars, 20 μm.

IFN, treatment led to robust ISG induction in the villous explants. The mechanistic basis for this differential signaling remains unknown but may reflect the constitutive expression of type III IFN already secreted by the syncytium during midgestation, which may affect receptor binding by the recombinant protein or perhaps reflect some level of receptor desensitization (*29*). Alternatively, it could also reflect the more restricted tissue expression of IFN-λ receptor, which is limited to the epithelium (*45*). However, midgestation explants express high basal levels of many ISGs, suggesting that the tissue is likely responsive to type III IFNs (*29*). Consistent with this, even in the placentas of mice that lack IFNAR and harbor high levels of virus in the placenta, the virus was mostly restricted from the fetus, indicating that other structures and pathways are capable of restricting ZIKV from the fetus.

How might type I IFNs trigger fetal death? We did not observe any differences in leukocyte infiltration into the placenta or block in proliferation of cells in the placenta. However, we did observe apoptosis of cells in the labyrinth, which likely represented endothelial cells or adjacent trophoblasts. Consistent with this, human explants treated with IFN-β exhibited significant alterations in actin cytoskeletal structure, consistent with cellular damage. These results are consistent with a previous report showing similar placenta damage after ZIKV infection (*13*). In addition to these possibilities, type I IFN is also known to inhibit angiogenesis and blood vessel development (*46*) and is consistent with the abnormal and reduced fetal blood vessels we observed in the labyrinth. Another possibility is that IFN may impair trophoblast fusion or differentiation. A previous report showed that IFN-β suppresses syncitin-1 expression (*47*). Consistent with this hypothesis, the placental histology and timing of death of the *Ifnar1*$^{+/-}$ fetuses resemble those of mice lacking syncitin-A, which have a defect in trophoblast fusion (*36*). We speculate that type I IFNs may serve as a quality control system to eliminate the developing embryo if coincident viral infection is detected and the levels of circulating IFNs reach a certain threshold. Many mammals carry their fetus for a prolonged period, to upward of ~650 days in elephants. This costly investment by the mothers may justify high levels of scrutiny of the health of the fetus at every level but particularly early in pregnancy when the embryo is vulnerable to various stressors (*48*, *49*). Type I IFNs may report on the viral infection status of the mother or the fetus within the local milieu, sending abortive signals to terminate pregnancy.

The effects of IFN on the developing placenta likely have implications for pregnancy complications beyond ZIKV, and it could be a

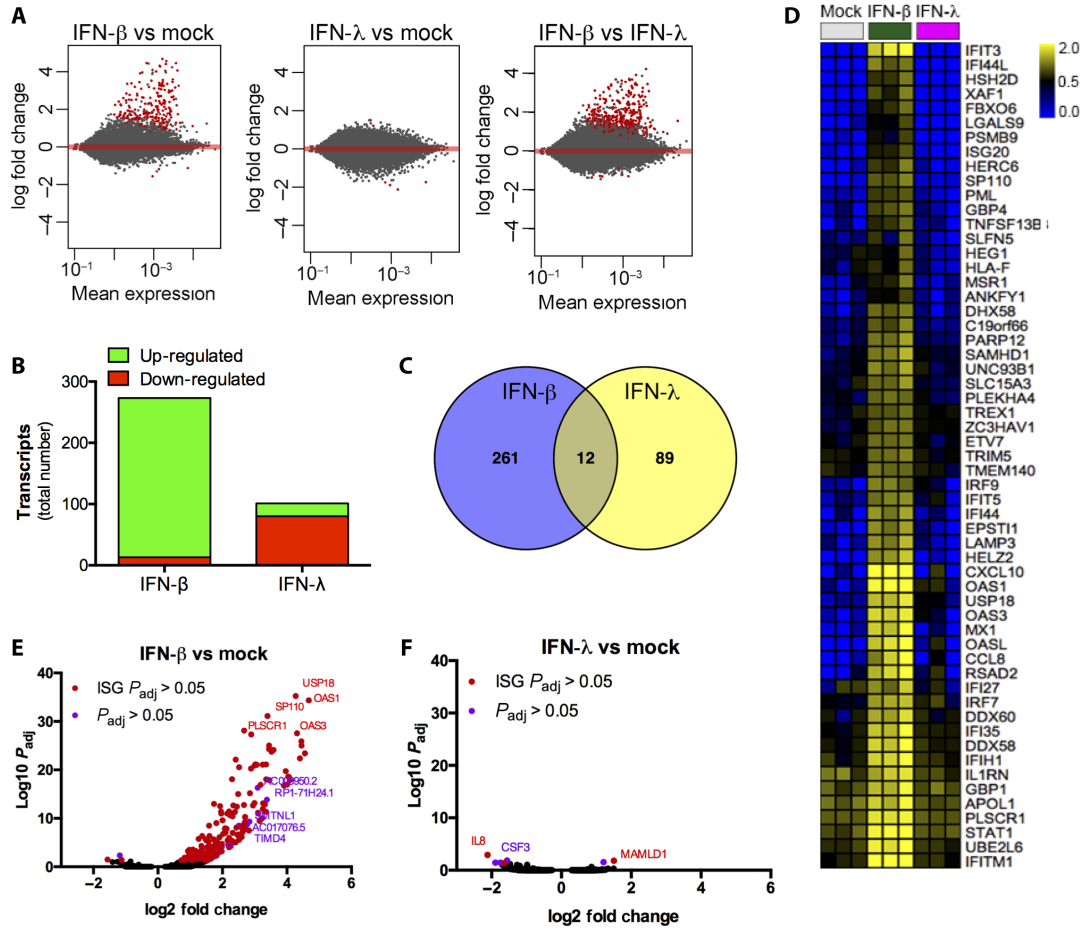

Fig. 8. ISGs are induced in IFN-β–treated villous explants. Human midgestation (19 to 23 weeks) chorionic villi were isolated, placed in culture, and treated with 1000 U of recombinant human IFN-β or 1000 U of IFN-λ3 for ~24 hours, and RNA was extracted. (**A**) MA plots generated in R after DeSeq2 analysis demonstrating the differential expression between IFN-β–treated (left) or IFN-λ–treated (middle) villi relative to mock-treated controls and between IFN-β– and IFN-λ–treated villi (right). Data are plotted as $\log_2$ fold changes (*y* axis) and mean expression (*x* axis). Red symbols denote transcripts whose expression was differentially expressed at $P < 0.05$. (**B**) Graph demonstrating the number of transcripts up-regulated (in green) or down-regulated (in red) after IFN-β or IFN-λ treatment of villi. (**C**) Venn diagram denoting the overlap of transcripts (12 in total) between villi treated with IFN-β and those treated with IFN-λ. (**D**) Heat map (based on log reads per kilobase of transcript per million mapped reads values) of known ISGs from mock-, IFN-β–, or IFN-λ–treated villi. (**E** and **F**) Volcano plots of villi treated with IFN-β (E) or IFN-λ (F) denoting specific ISGs differentially expressed by treatment. Red circles denote ISGs and purple circles denote non-ISG transcripts. For RNA-seq experiments, data represent villi isolated from three independent placental preparations.

mechanism for adverse pregnancy outcomes, such as IUGR or early spontaneous abortions, which often occur without a known underlying etiology. Consistent with type I IFN being an underlying cause of pregnancy complications, many congenital or "TORCH" (Toxoplasmosis, Other, Rubella, Cytomegalovirus, and Herpes) infections have a common presentation of microcephaly, cerebral calcifications, and IUGR (*3*). Beyond viral infections, our study may be relevant to diseases in which type I IFNs are overproduced, collectively known as interferonopathies (*50*). Interferonopathies may be induced by monogenic mutations, such as those found in Aicardi-Goutières syndrome, or polygenic diseases, including systemic lupus erythematosus (SLE). Fetuses with Aicardi-Goutières syndrome can present with developmental defects similar to classic TORCH infection with fetal growth restriction, microcephaly, and intracerebral calcifications (*50*). SLE is associated with pregnancy complications, including fetal death in utero, preeclampsia, and preterm birth; and elevated serum IFN is one of the key factors that closely correlate with poor pregnancy outcomes (*51*). Our study implicates type I IFNs as a possible common culprit for virus-associated pregnancy complications and suggests blockade of type I IFNs as a possible intervention to prevent pregnancy complications in the settings of nonviral interferonopathies.

MATERIALS AND METHODS

Study design

To test the effect that fetal IFNAR signaling has on development after ZIKV infection, *Ifnar1*$^{-/-}$ females were crossed to *Ifnar1*$^{+/-}$ males to allow for direct comparison between littermates of different genotypes. Fetuses and placentas were harvested at various time points after infection and appearance, histology, and transcriptional changes were analyzed. To test how human placentas were affected by IFN signaling, midgestation chorionic villous explants were treated with IFN-β or IFN-λ, and villi were analyzed by immunofluorescent imaging or transcriptional changes were analyzed. For mouse studies, analysis was performed on litters containing both genotypes, and genotyping of litters was performed after initial analysis of fetal weight and appearance. No other formal randomization or blinding method was used. Subjects were assigned a litter and fetus number to allow unbiased selection for sample processing (RNA and imaging). A minimum of three infected litters were analyzed per time point. Exact *n* is indicated in figure legends. No formal statistical tool was used to determine power.

Mice

Ifnar1$^{-/-}$, *Ifnar1*$^{+/-}$, C57BL/6, and *Irf3*$^{-/-}$*Irf7*$^{-/-}$ mice were bred and maintained at Yale University. All pregnant dams were between 9 and

20 weeks of age. Littermates were randomly assigned to infected or uninfected groups. *Ifnar1*$^{+/-}$ male breeders are the F1 generation from cross between C57BL/6 (B6) and *Ifnar1*$^{-/-}$ parents. Matings were timed by checking for the presence of a vaginal plug, indicating gestational age E0.5. About 11% of infected concepti were analyzed between E9.5 and E12.5 and 17% of uninfected concepti developed into abnormal spheroid shapes (distinct from infection-induced resorbed fetuses), without the presence of a fetus or yolk sac. These were excluded from analysis because of inability to obtain adequate fetus-derived tissue for genotyping analysis and because it was present in equal frequencies for infected and uninfected groups. All animal procedures were performed in compliance with Yale Institutional Animal Care and Use Committee protocols.

Midgestation chorionic villous explants

Human fetal placental tissue from 19 to 23 weeks' gestation that resulted from elective terminations was obtained from the University of Pittsburgh Health Sciences Tissue Bank through an honest broker system after approval from the University of Pittsburgh Institutional Review Board and in accordance with the University of Pittsburgh anatomical tissue procurement guidelines. Chorionic villi (about 1 cm × 1 cm in size) were dissected and cultured in Dulbecco's modified Eagle's medium (DMEM)/F12 (1:1) supplemented with 10% fetal bovine serum (FBS), penicillin/streptomycin, and amphotericin B. Immediately after isolation, isolated villi were treated with the indicated dose of recombinant IFN-β or IFN-λ for 24 hours, and then tissue was fixed and processed for imaging. For imaging studies, villi were fixed in 4% paraformaldehyde (PFA) followed by permeabilization in 0.25% Triton X-100 for 30 min at room temperature with gentle agitation, washed in phosphate-buffered saline (PBS), incubated with primary antibody, washed again in PBS, and then incubated with Alexa Fluor–conjugated secondary antibodies. Alexa Fluor–conjugated phalloidin was purchased from Invitrogen (A12379 or A12381). Rabbit anti-CK19 (ab52625) was purchased from Abcam. After staining, villi were mounted with VECTASHIELD (Vector Laboratories) containing 4′,6-diamidino-2-phenylindole (DAPI), and images were captured using an Olympus FV1000 confocal or Zeiss LSM 710 confocal microscope. Images were adjusted for brightness/contrast using Adobe Photoshop (Adobe), and syncytial knot size was calculated using Imaris.

Viruses and in vivo infections

ZIKV Cambodian FSS13025 stain, obtained from the World Reference Center for Emerging Viruses and Arboviruses at University of Texas Medical Branch, Galveston, was used for intravaginal infection studies. Stocks were propagated in Vero cells and titrated by plaque assay as previously described (*14*). ZIKV Brazilian PE243, used for subcutaneous infections, was recovered from a 19-year-old female in Brazil from 2015 (*52*). Vero cells were obtained from the American Type Culture Collection. Cell lines were verified by morphology and were tested for mycoplasma contamination every 1 to 2 years.

Intravaginal infection was performed as previously described: At E5.5 or E8.5, a calginate swab (Fischer Scientific) was used to remove mucus from the vaginal lumen, and 1.5×10^5 PFU of ZIKV was inoculated into the vagina using a pipette (*14*). Subcutaneous infection was performed by injecting 100 μl of virus stock diluted in PBS (3.4×10^5 or 1×10^3 PFU) into the footpad. Pregnant mice were euthanized, tissues were harvested at indicated time points, and fetuses and placentas were either collected in TRIzol (for RNA extraction), fixed in 4% PFA (for imaging), or collected in DMEM with 10% FBS and penicillin/streptomycin (for plaque assay). Fixed fetuses were imaged using a Zeiss Discovery V8 stereomicroscope (Zeiss). Yolk sac for E9.5 to E12.5 or tail for E17.5 fetuses was collected for each fetus and genotyped using the following primers: ATTATTAAAAGAAAAGACGAGGCGAAGTGG (forward) and AAGATGTGCTGTTCCCTTCCTCTGCTCTGA (reverse), with a 150–base pair product, indicating the presence of a WT copy of IFNAR.

Poly(I:C) challenge

Two hundred micrograms of HMW VacciGrade Poly(I:C) (InvivoGen) was injected intraperitoneally into pregnant mice at E7.5. Mice were then harvested between E9.5 and E12.5 to examine fetuses.

Quantification of ZIKV genome, ISGs, and hypoxia response genes by qRT-PCR

Tissues were extracted using TRIzol (Thermo Fischer Scientific) and purified using an RNeasy Mini Kit (Qiagen). iScript cDNA synthesis kit (Bio-Rad) was used to synthesize cDNA. Quantitative polymerase chain reaction (qPCR), which was performed using SYBR green (Bio-Rad), was used to quantify ZIKV levels, ISGs, and hypoxia response genes and ran on a CFX Connect instrument (Bio-Rad). Primer sequences are provided in table S1. Virus and ISGs were normalized to *Hprt* (*14*).

Histology, immunofluorescence, and immunohistochemistry staining of mouse placentas

Placentas were fixed in 4% PFA overnight at 4°C. For immunohistochemical (IHC) and hematoxylin and eosin (H&E) staining, tissues were embedded in paraffin blocks and sectioned by the Yale Pathology Tissue Services. H&E was performed by the Yale Pathology Tissue Services. For IHC, paraffin sections were heated for 30 min at 55° to 60°C. Antigen retrieval was performed by boiling in sodium citrate (J.T. Baker) (pH 6.0) for 60 min. Blocking was performed using PBS (AmericanBio), 1% bovine serum albumin (BSA) (Sigma-Aldrich), and 0.5% Tween 20 (Sigma-Aldrich) adjusted to pH 7.4. Slides were stained for CD31 (goat, 1:1000, R&D AF3628), Casp3 (rabbit, 1:1000, Cell Signaling Tech 9664T), Ecad (1:500, Thermo Fischer Scientific 13-1900), and Ki67 (rabbit 1:1000, Cell Signaling Tech 12202T) at 4°C overnight. Slides were blocked with Bloxall (Vector Laboratories) and stained with rat (for Ecad), rabbit (for Casp3, Ki67), or goat (for CD31) ImmPRESS antibodies (Vector Laboratories) and 3,3′-diaminobenzidine (DAB) (Vector Laboratories) per the manufacturer's instructions. For immunofluorescence staining, slides were embedded in optimal cutting temperature media (Tissue Tek). Five- to seven-micrometer frozen sections were cut using a cryostat, and sections were allowed to dry at room temperature. Sections were blocked with 2% normal Donkey serum (Jackson ImmunoResearch) in PBS with Tween 20 and 1% BSA (Sigma-Aldrich) and stained with ZIKV-immune rat serum (*53*), CD45 (R&D Systems AF114), CK (Dako Z0622), or CD31 (R&D Systems AF3628) overnight at room temperature. Sections were then stained with A488 anti-rat secondary (Thermo Fischer), A647 anti-rabbit (Thermo Fischer), Cy3 anti-rabbit (Jackson ImmunoResearch), A488 anti-goat (Thermo Fischer), or NL557 anti-goat (R&D Systems). Samples were stained with DAPI and mounted with ProLong Diamond Antifade Mountant (Molecular Probes). H&E and IHC images were captured using light microscopy (BX51; Olympus), and immunofluorescence images were captured using fluorescence microscopy (BX51; Olympus) or confocal microscopy (TCS SP2; Leica). Images were merged and brightness and contrast were adjusted using ImageJ.

Transmission electron microscopy of mouse placentas

Placentas were fixed in formaldehyde/glutaraldehyde 2.5% in phosphate buffer for at least 24 hours. Samples were washed and secondarily fixed in osmium tetroxide; negative staining was performed with uranyl acetate, treated in ascending alcohols, and finally embedded in Durcupan ACM (EMS 14040). Ultrathin sections (70 nM) were cut on a Leica ultramicrotome, collected on Formvar-coated grids, and analyzed on a Tecnai 12 FEI electron microscope.

RNA-seq and qRT-PCR analysis of midgestation chorionic villous explants

RNA was isolated from the villous explants using GenElute RNA total RNA miniprep kit (Sigma-Aldrich) and treated with deoxyribonuclease (Sigma-Aldrich). For RNA-seq, as previously described (*28*, *54*), libraries were prepared using New England Biolabs Ultra Library Preparation kit. An Illumina HiSeq2500 was used for sequencing, and CLC Genomics Workbench 9.0 (Qiagen) was used to process, normalize, and map sequence data to the human reference genome (hg19). DESeq2 in R (*55*) or CLC Genomics Workbench 9 was used to identify differentially expressed genes and to generate MA plots.

Statistical analysis

In all analyses except for RNA-seq, data analysis was performed using Microsoft Excel and GraphPad Prism. Exact statistical test and value of *n* are detailed in the figure legends. A Tukey's multiple comparison test or Dunnett's multiple comparison test was used to determine significance when determining significance between multiple groups (>3). A paired Student's *t* test was used when comparing only two groups. *t* tests assumed a normal distribution for all samples and *t* tests assume an unequal standard deviation and variance between groups.

SUPPLEMENTARY MATERIALS

immunology.sciencemag.org/cgi/content/full/3/19/eaao1680/DC1

Methods

Fig. S1. ISG expression is elevated in *Ifnar1*$^{+/-}$ placentas and fetuses but not in *Irf3*$^{-/-}$*Irf7*$^{-/-}$ after ZIKV infection.

Fig. S2. *Ifnar1*$^{-/-}$ placentas harbor more infectious ZIKV compared with *Ifnar1*$^{+/-}$ littermates.

Fig. S3. Global gene expression analysis reveals elevated ISG levels in infected *Ifnar1*$^{+/-}$ placentas.

Fig. S4. ZIKV infection of the maternal-fetal interface is restricted to the decidua.

Fig. S5. Placental architecture of *Ifnar1*$^{+/-}$ fetuses is normal at E9.5 but disrupted at E11.5 and E12.5.

Fig. S6. Labyrinth of *Ifnar1*$^{+/-}$ placenta exhibits decreased fetal endothelial cells.

Fig. S7. *Ifnar1*$^{+/-}$ but not *Ifnar1*$^{-/-}$ fetuses are resorbed after subcutaneous infection with Brazilian ZIKV.

Table S1. Primers for mouse qPCR

Table S2. Top differentially regulated genes and pathways in ZIKV-infected *Ifnar1*$^{+/-}$ versus *Ifnar1*$^{-/-}$ placentas.

Table S3. Individual values included in all graphs

References (*56*–*61*)

REFERENCES AND NOTES

1. Pan American Health Organization/World Health Organization, Zika suspected and confirmed cases reported by countries and territories in the Americas Cumulative cases, 2015-2016 (Washington, D.C., 2016).
2. D. Baud, D. J. Gubler, B. Schaub, M. C. Lanteri, D. Musso, An update on Zika virus infection. *Lancet* **390**, 2099–2109 (2017).
3. C. B. Coyne, H. M. Lazear, Zika virus—Reigniting the TORCH. *Nat. Rev. Microbiol.* **14**, 707–715 (2016).
4. L. Barzon, M. Pacenti, E. Franchin, E. Lavezzo, M. Trevisan, D. Sgarabotto, G. Palù, Infection dynamics in a traveller with persistent shedding of Zika virus RNA in semen for six months after returning from Haiti to Italy, January 2016. *Euro Surveill.* **21**, 30316 (2016).
5. E. D'Ortenzio, S. Matheron, Y. Yazdanpanah, X. de Lamballerie, B. Hubert, G. Piorkowski, M. Maquart, D. Descamps, F. Damond, I. Leparc-Goffart, Evidence of sexual transmission of Zika virus. *N. Engl. J. Med.* 2195–2198 (2016).
6. A. J. Sadler, B. R. G. Williams, Interferon-inducible antiviral effectors. *Nat. Rev. Immunol.* **8**, 559–568 (2008).
7. O. Takeuchi, S. Akira, Recognition of viruses by innate immunity. *Immunol. Rev.* **220**, 214–224 (2007).
8. K. Honda, T. Taniguchi, IRFs : Master regulators of signalling by Toll-like receptors and cytosolic pattern-recognition receptors. *Nat. Rev. Immunol.* **6**, 644–658 (2006).
9. J. W. Schoggins, C. M. Rice, Interferon-stimulated genes and their antiviral effector functions. *Curr. Opin. Virol.* **1**, 519–525 (2011).
10. J. Crouse, U. Kalinke, A. Oxenius, Regulation of antiviral T cell responses by type I interferons. *Nat. Rev. Immunol.* **15**, 231–242 (2015).
11. M. Chawla-Sarkar, D. J. Lindner, Y.-F. Liu, B. R. Williams, G. C. Sen, R. H. Silverman, E. C. Borden, Apoptosis and interferons: Role of interferon-stimulated genes as mediators of apoptosis. *Apoptosis* **8**, 237–249 (2003).
12. F. R. Cugola, I. R. Fernandes, F. B. Russo, B. C. Freitas, J. L. M. Dias, K. P. Guimarães, C. Benazzato, N. Almeida, G. C. Pignatari, S. Romero, C. M. Polonio, I. Cunha, C. L. Freitas, W. N. Brandão, C. Rossato, D. G. Andrade, D. de P. Faria, A. T. Garcez, C. A. Buchpigel, C. T. Braconi, E. Mendes, A. A. Sall, P. M. de A. Zanotto, J. P. S. Peron, A. R. Muotri, P. C. B. Beltrão, The Brazilian Zika virus strain causes birth defects in experimental models. *Nature* **534**, 267–271 (2016).
13. J. J. Miner, B. Cao, J. Govero, A. M. Smith, E. Fernandez, O. H. Cabrera, C. Garber, M. Noll, R. S. Klein, K. K. Noguchi, I. U. Mysorekar, M. S. Diamond, Zika virus infection during pregnancy in mice causes placental damage and fetal demise. *Cell* **165**, 1081–1091 (2016).
14. L. J. Yockey, L. Varela, T. Rakib, W. Khoury-Hanold, S. L. Fink, B. Stutz, K. Szigeti-Buck, A. Van den Pol, B. D. Lindenbach, T. L. Horvath, A. Iwasaki, Vaginal exposure to Zika virus during pregnancy leads to fetal brain infection. *Cell* **166**, 1247–1256.e4 (2016).
15. J. Xavier-Neto, M. Carvalho, B. dos Santos Pascoalino, A. C. Cardoso, Â. M. S. Costa, A. H. M. Pereira, L. N. Santos, Â. Saito, R. E. Marques, J. H. C. Smetana, S. R. Consonni, C. Bandeira, V. V. Costa, M. C. Bajgelman, P. S. Lopes de Oliveira, M. T. Cordeiro, L. H. V. G. Gil, B. A. Pauletti, D. C. Granato, A. F. P. Leme, L. Freitas-Junior, C. B. M. Holanda de Freitas, M. M. Teixeira, E. Bevilacqua, K. Franchini, Hydrocephalus and arthrogryposis in an immunocompetent mouse model of ZIKA teratogeny: A developmental study. *PLOS Neglected Trop. Dis.* **11**, e0005363 (2017).
16. C. W. Winkler, T. A. Woods, R. Rosenke, D. P. Scott, S. M. Best, K. E. Peterson, Sexual and vertical transmission of Zika virus in anti-interferon receptor-treated Rag-1deficient mice. *Sci. Rep.* **7**, 7176 (2017).
17. A. Grant, S. S. Ponia, S. Tripathi, V. Balasubramaniam, L. Miorin, M. Sourisseau, M. C. Schwarz, M. P. Sánchez-Seco, M. J. Evans, S. M. Best, A. García-Sastre, Zika virus targets human STAT2 to inhibit type I interferon signaling. *Cell Host Microbe* **19**, 882–890 (2016).
18. Y. Wu, Q. Liu, J. Zhou, W. Xie, C. Chen, Z. Wang, H. Yang, J. Cui, Zika virus evades interferon-mediated antiviral response through the co-operation of multiple nonstructural proteins in vitro. *Cell Discov.* **3**, 17006 (2017).
19. H. M. Lazear, J. Govero, A. M. Smith, D. J. Platt, E. Fernandez, J. J. Miner, M. S. Diamond, A mouse model of Zika virus pathogenesis. *Cell Host Microbe* **19**, 720–730 (2016).
20. B. W. Jagger, J. J. Miner, B. Cao, N. Arora, A. M. Smith, A. Kovacs, I. U. Mysorekar, C. B. Coyne, M. S. Diamond, Gestational stage and IFN- λ signaling regulate ZIKV infection in utero. *Cell Host Microbe* **22**, 366–376.e3 (2017).
21. J. R. Robbins, A. I. Bakardjiev, Pathogens and the placental fortress. *Curr. Opin. Microbiol.* **15**, 36–43 (2012).
22. T. Cotechini, C. H. Graham, Aberrant maternal inflammation as a cause of pregnancy complications: A potential therapeutic target? *Placenta* **36**, 960–966 (2015).
23. M. Prabhudas, E. Bonney, K. Caron, S. Dey, A. Erlebacher, A. Fazleabas, S. Fisher, T. Golos, M. Matzuk, J. M McCune, G. Mor, L. Schulz, M. Soares, T. Spencer, J. Strominger, S. S. Way, K. Yoshinaga, Immune mechanisms at the maternal-fetal interface : Perspectives and challenges. *Nat. Immunol.* **16**, 328–334 (2015).
24. G. Mor, Placental inflammatory response to Zika virus may affect fetal brain development. *Am. J. Reprod. Immunol.* **75**, 421–422 (2016).
25. M. Cappelletti, P. Presicce, M. J. Lawson, V. Chaturvedi, T. E. Stankiewicz, S. Vanoni, I. T. W. Harley, J. W. McAlees, D. A. Giles, M. E. Moreno-Fernandez, C. M. Rueda, P. Senthamaraikannan, X. Sun, R. Karns, K. Hoebe, E. M. Janssen, C. L. Karp, D. A. Hildeman, S. P. Hogan, S. G. Kallapur, C. A. Chougnet, S. S. Way, S. Divanovic, Type I interferons regulate susceptibility to inflammation-induced preterm birth. *JCI Insight* **2**, e91288 (2017).
26. K. Racicot, P. Aldo, A. El-guindy, J.-Y. Kwon, R. Romero, G. Mor, Cutting edge: Fetal/placental type I IFN can affect maternal survival and fetal viral load during viral infection. *J. Immunol.* **198**, 3029–3032 (2017).
27. R. M. Roberts, Interferon-tau, a type 1 interferon involved in maternal recognition of pregnancy. *Cytokine Growth Factor Rev.* **18**, 403–408 (2007).

28. A. Bayer, N. J. Lennemann, Y. Ouyang, J. C. Bramley, S. Morosky, E. Torres De Azeved Marques Jr., S. Cherry, Y. Sadovsky, C. B. Coyne, Type III interferons produced by human placental trophoblasts confer protection against Zika virus infection. *Cell Host Microbe* **19**, 705–712 (2016).
29. J. Corry, N. Arora, C. A. Good, Y. Sadovsky, C. B. Coyne, Organotypic models of type III interferon-mediated protection from Zika virus infections at the maternal–fetal interface. *Proc. Natl. Acad. Sci. U.S.A.* **114**, 9433–9438 (2017).
30. J. L. Sones, R. L. Davisson, Preeclampsia, of mice and women. *Physiol. Genomics* **48**, 565–572 (2016).
31. V. E. Papaioannou, R. R. Behringer, Early embryonic lethality in genetically engineered mice: Diagnosis and phenotypic analysis. *Vet. Pathol.* **49**, 64–70 (2012).
32. P. M. Coan, A. C. Ferguson-Smith, G. J. Burton, Ultrastructural changes in the interhaemal membrane and junctional zone of the murine chorioallantoic placenta across gestation. *J. Anat.* **207**, 783–796 (2005).
33. J. Rossant, J. C. Cross, Placental development: Lessons from mouse mutants. *Nat. Rev. Genet.* **2**, 538–548 (2001).
34. M. Mori, A. Bogdan, T. Balassa, T. Csabai, J. Szekeres-Bartho, The decidua—the maternal bed embracing the embryo—maintains the pregnancy. *Semin. Immunopathol.* **38**, 635–649 (2016).
35. J. Bhatnagar, D. B. Rabeneck, R. B. Martines, S. Reagan-Steiner, Y. Ermias, L. B. C. Estetter, T. Suzuki, J. M. Ritter, M. K. Keating, G. Hale, J. Gary, A. Muehlenbachs, A. J. Lambert, R. Lanciotti, T. Oduyebo, D. Meaney-Delman, F. Bolaños, E. A. Parra Saad, W.-J. Shieh, S. R. Zaki, Zika virus RNA replication and persistence in brain and placenta tissue. *Emerg. Infect. Dis.* **23**, 405–414 (2017).
36. A. Dupressoir, C. Vernochet, O. Bawa, F. Harper, G. Pierron, P. Opolon, T. Heidmann, Syncytin-A knockout mice demonstrate the critical role in placentation of a fusogenic, endogenous retrovirus-derived, envelope gene. *Proc. Natl. Acad. Sci. U.S.A.* **106**, 12127–12132 (2009).
37. M. Ream, A. M. Ray, R. Chandra, D. M. Chikaraishi, Early fetal hypoxia leads to growth restriction and myocardial thinning. *Am. J. Physiol. Regul. Integr. Comp. Physiol.* **295**, R583–R595 (2008).
38. R. Trollmann, H. Rehrauer, C. Schneider, G. Krischke, N. Huemmler, S. Keller, W. Rascher, M. Gassmann, Late-gestational systemic hypoxia leads to a similar early gene response in mouse placenta and developing brain. *Am. J. Physiol.* **299**, R1489–R1499 (2010).
39. M. Matsumoto, T. Seya, TLR3: Interferon induction by double-stranded RNA including poly(I:C). *Adv. Drug Deliv. Rev.* **60**, 805–812 (2008).
40. J. E. Thaxton, T. Nevers, E. O. Lippe, S. M. Blois, S. Saito, S. Sharma, NKG2D blockade inhibits poly(I:C)-triggered fetal loss in wild type but not IL-10$^{-/-}$ mice. *J. Immunol.* **190**, 3639–3647 (2013).
41. G. J. Burton, C. J. P. Jones, Syncytial knots, sprouts, apoptosis, and trophoblast deportation from the human placenta. *Taiwan. J. Obstet. Gynecol.* **48**, 28–37 (2009).
42. N. M. E. Fogarty, A. C. Ferguson-Smith, G. J. Burton, Syncytial knots (Tenney-Parker changes) in the human placenta: Evidence of loss of transcriptional activity and oxidative damage. *Am. J. Pathol.* **183**, 144–152 (2013).
43. R. Uraki, K. A. Jurado, J. Hwang, K. Szigeti-Buck, T. L. Hovarth, A. Iwasaki, E. Fikrig, Fetal growth restriction caused by sexual transmission of Zika virus in mice. *J. Infect. Dis.* **215**, 1720–1724 (2017).
44. K. Loukeris, R. Sela, R. N. Baergen, Syncytial knots as a reflection of placental maturity: Reference values for 20 to 40 weeks' gestational age. *Pediatr. Dev. Pathol.* **13**, 305–309 (2010).
45. C. Odendall, J. C. Kagan, The unique regulation and functions of type III interferons in antiviral immunity. *Curr. Opin. Virol.* **12**, 47–52 (2015).
46. R. A. B. Ezekowitc, J. B. Mulliken, J. Folkman, Interferon Alfa-2a therapy for life-threatening hemangiomas of infancy. *N. Engl. J. Med.* **326**, 1456–1463 (1992).
47. G. Mameli, A. Dolei, V. Astone, K. Khalili, C. Serra, B. E. Sawaya, Regulation of the syncytin-1 promoter in human astrocytes by multiple sclerosis-related cytokines. *Virology* **362**, 120–130 (2007).
48. G. Teklenburg, M. Salker, M. Molokhia, S. Lavery, G. Trew, T. Aojanepong, H. J. Mardon, A. U. Lokugamage, R. Rai, C. Landles, B. A. J. Roelen, S. Quenby, E. W. Kuijk, A. Kavelaars, C. J. Heijnen, L. Regan, J. J. Brosens, N. S. Macklon, Natural selection of human embryos: Decidualizing endometrial stromal cells serve as sensors of embryo quality upon implantation. *PLOS ONE* **5**, e10258 (2010).
49. E. C. Larsen, O. B. Christiansen, A. M. Kolte, N. Macklon, New insights into mechanisms behind miscarriage. *BMC Med.* **11**, 154 (2013).
50. Y. J. Crow, Type I interferonopathies : A novel set of inborn errors of immunity. *Ann. N.Y. Acad. Sci.* **1238**, 91–98 (2011).
51. D. Andrade, M. Kim, L. P. Blanco, S. A. Karumanchi, G. C. Koo, P. Redecha, K. Kirou, A. M. Alvarez, M. J. Mulla, M. K. Crow, V. M. Abrahams, M. J. Kaplan, J. E. Salmon, Interferon-α and angiogenic dysregulation in pregnant lupus patients who develop preeclampsia. *Arthritis Rheumatol.* **67**, 977–987 (2015).
52. M. Onorati, Z. Li, F. Liu, A. M. M. Sousa, N. Nakagawa, M. Li, M. T. Dell'Anno, F. O. Gulden, S. Pochareddy, A. T. N. Tebbenkamp, W. Han, M. Pletikos, T. Gao, Y. Zhu, C. Bichsel, L. Varela, K. Szigeti-Buck, S. Lisgo, Y. Zhang, A. Testen, X.-B. Gao, J. Mlakar, M. Popovic, M. Flamand, S. M. Strittmatter, L. K. Kaczmarek, E. S. Anton, T. L. Horvath, B. D. Lindenbach, N. Sestan, Zika virus disrupts phospho-TBK1 localization and mitosis in human neuroepithelial stem cells and radial glia. *Cell Rep.* **16**, 2576–2592 (2016).
53. A. N. van den Pol, G. Mao, Y. Yang, S. Ornaghi, J. N. Davis, Zika virus targeting in the developing brain. *J. Neurosci.* **37**, 2161–2175 (2017).
54. C. A. Mcconkey, E. Delorme-Axford, C. A. Nickerson, K. S. Kim, Y. Sadovsky, J. P. Boyle, C. B. Coyne, A three-dimensional culture system recapitulates placental syncytiotrophoblast development and microbial resistance. *Sci. Adv.* **2**, e1501462 (2016).
55. M. I. Love, W. Huber, S. Anders, Moderated estimation of fold change and dispersion for RNA-seq data with DESeq2. *Genome Biol.* **15**, 550 (2014).
56. Y. Kong, Btrim: A fast, lightweight adapter and quality trimming program for next-generation sequencing technologies. *Genomics* **98**, 152–153 (2011).
57. D. Kim, G. Pertea, C. Trapnell, H. Pimentel, R. Kelley, S. L. Salzberg, TopHat2: Accurate alignment of transcriptomes in the presence of insertions, deletions and gene fusions. *Genome Biol.* **14**, R36 (2013).
58. A. Subramanian, P. Tamayo, V. K. Mootha, S. Mukherjee, B. L. Ebert, M. A. Gillette, A. Paulovich, S. L. Pomeroy, T. R. Golub, E. S. Lander, J. P. Mesirov, Gene set enrichment analysis: A knowledge-based approach for interpreting genome-wide expression profiles. *Proc. Natl. Acad. Sci. U.S.A.* **102**, 15545–15550 (2005).
59. V. K. Mootha, C. M. Lindgren, K.-F. Eriksson, A. Subramanian, S. Sihag, J. Lehar, P. Puigserver, E. Carlsson, M. Ridderstråle, E. Laurila, N. Houstis, M. J. Daly, N. Patterson, J. P. Mesirov, T. R. Golub, P. Tamayo, B. Spiegelman, E. S. Lander, J. N. Hirschhorn, D. Altshuler, L. C. Groop, PGC-1α-responsive genes involved in oxidative phosphorylation are coordinately downregulated in human diabetes. *Nat. Genet.* **34**, 267–273 (2003).
60. E. F. Foxman, J. A. Storer, M. E. Fitzgerald, B. R. Wasike, L. Houf, H. Zhaof, P. E. Turnere, A. Marie Pyle, A. Iwasaki, Temperature-dependent innate defense against the common cold virus limits viral replication at warm temperature in mouse airway cells. *Proc. Natl. Acad. Sci. U.S.A.* **112**, 827–832 (2014).
61. V. C. Thompson, T. K. Day, T. Bianco-Miotto, L. A. Selth, G. Han, M. Thomas, G. Buchanan, H. I. Scher, C. C. Nelson; Australian Prostate Cancer BioResource, N. M. Greenberg, L. M. Butler, W. D. Tilley, A gene signature identified using a mouse model of androgen receptor-dependent prostate cancer predicts biochemical relapse in human disease. *Int. J. Cancer* **131**, 662–672 (2012).

Acknowledgments: We thank B. Lindenbach for providing ZIKV stocks, A. Van den Pol for providing the ZIKV antibody, R. Medzhitov for mice, H. Dong and M. Linehan for technical assistance, and the University of Pittsburgh Medical Center Tissue and Research Pathology Services/Health Sciences Tissue Bank, which receives funding from P30CA047904. **Funding:** This study was supported in part by the NIH (1R21AI131284 to A.I., T32GM007205 and F30 HD094717-01 to L.J.Y., 4T32AI007019-41 to K.A.J, and R01HD075665 to C.B.C) and a Burroughs Wellcome Investigators in the Pathogenesis of Infectious Disease Award to C.B.C. K.A.J. is a recipient of the Burroughs Wellcome Fund Postdoctoral Enrichment Program. A.I. and E.F. are investigators of the Howard Hughes Medical Institute. **Author contributions:** Conceptualization and methodology: L.J.Y., K.A.J., N.A., K.M.M., Y.K., S.W., H.J.K., C.B.C., and A.I. Investigation: L.J.Y., K.A.J., N.A., T.R., and A.K.H. Formal analysis: L.J.Y., K.A.J., N.A., A.M., Y.K., S.W., H.J.K., C.B.C., and A.I. Resources: E.F., T.L.H. Writing: L.J.Y., N.A., C.B.C., and A.I. (original draft), and L.J.Y., K.A.J., N.A., A.M., A.J.K., E.F., S.W., H.J.K., C.B.C., and A.I. (review and editing). Funding acquisition: C.B.C. and A.I. Supervision: S.W., H.K.J., C.B.C., and A.I. **Competing interests:** The authors declare that they have no competing interests. **Data and materials availability:** Data from RNA-seq analysis are available through the GEO database [accession numbers GSE98423 (mouse placentas; fig S3 and table S2) and GSE104349 (human chorionic villi; Fig.7)].

Submitted 21 June 2017
Accepted 2 November 2017
Published 5 January 2018
10.1126/sciimmunol.aao1680

Citation: L. J. Yockey, K. A. Jurado, N. Arora, A. Millet, T. Rakib, K. M. Milano, A. K. Hastings, E. Fikrig, Y. Kong, T. L. Horvath, S. Weatherbee, H. J. Kliman, C. B. Coyne, A. Iwasaki, Type I interferons instigate fetal demise after Zika virus infection. *Sci. Immunol.* **3**, eaao1680 (2018).

Science Immunology

Type I interferons instigate fetal demise after Zika virus infection

Laura J. Yockey, Kellie A. Jurado, Nitin Arora, Alon Millet, Tasfia Rakib, Kristin M. Milano, Andrew K. Hastings, Erol Fikrig, Yong Kong, Tamas L. Horvath, Scott Weatherbee, Harvey J. Kliman, Carolyn B. Coyne and Akiko Iwasaki

Sci. Immunol. **3**, eaao1680.
DOI: 10.1126/sciimmunol.aao1680

The interferon boomerang

Interferon-α/β receptor (IFNAR) –deficient mice are highly susceptible to viruses, including Zika virus (ZIKV). Previous studies modeled ZIKV infection during pregnancy in mice by crossing *Ifnar1*$^{-/-}$ females to wild-type males, generating *Ifnar1*$^{+/-}$ fetuses that retain type I interferon (IFN) responsiveness. Yockey *et al.* have directly examined the role of fetal type I IFN signaling in protection in this context, by crossing *Ifnar1*$^{-/-}$ females to *Ifnar1*$^{+/-}$ males. Although *Ifnar1*$^{-/-}$ fetuses had higher ZIKV titers as compared with *Ifnar1*$^{+/-}$ fetuses, *Ifnar1*$^{-/-}$ fetuses survived longer. Furthermore, they found that activation of type I IFN signaling in the placentas of *Ifnar1*$^{+/-}$ fetuses led to fetal hypoxia, demise, and resorption. Beyond ZIKV infection, the study calls for closer examination of the role of IFNs in pregnancy-associated complications.